Searching for Lensed Gravitational Waves from Compact Binary Coalescences Final Report

Li Ka Yue Alvin[1]
Mentors: Alan J.Weinstein[2] and Surabhi Sachdev[2]

[1]Department of Physics, The Chinese University of Hong Kong
[2]LIGO Laboratory, California Institute of Technology

LIGO SURF 2018 Program, California Institute of Technology
Date : 24^{th} September, 2018

Einstein's general relativity predicts the radiation of gravitational waves when masses accelerate, for instance, as the components of a binary black hole system orbit each other. This was confirmed when LIGO (The Laser-Interferometry Gravitational-wave Observatory) made the first detection of gravitational waves from a binary black hole merger on 14 September 2015. The success of gravitational waves detection opens a new window for scientists to study the Universe. In Einstein's general theory of relativity, it is also predicted that light rays bend when passing by masses in spacetime, a phenomenon known as gravitational lensing. As a manifestation of Einstein's equivalence principle, everything in motion, independent of their nature, is gravitationally lensed in the same way. In such sense, gravitational waves will also be lensed, resulting in multiple signals which differ in arrival times and amplitudes. Since the amplitudes of such signals may differ, there are cases that they are not identified as signals. In this research, we aim to search for lensed signals of the binary black hole signals detected by LIGO. We generate templates of possible lensed gravitational wave signals for detected events by simulating gravitational wave signals as observed by LIGO. Our major objective is to make use of those templates in the reduced template bank to re-identify possible lensed signals which may have insufficiently high signal-to-noise ratio to be distinguishable from detector noise when a full template bank is used. We will further attempt to infer the intrinsic properties of the gravitational lenses from the lensed gravitational wave signals identified.

I. Introduction and Motivation

With the successful detections of gravitational waves [**?**], [**?**], [**?**], [**?**], [**?**], [**?**] over the past few years, we have already verified the existence of gravitational waves predicted by Albert Einstein's general theory of relativity in 1915 [**?**]. Therefore, it is now the right time to test the other properties of gravitational waves as General Relativity predicts, and in this project, our main focus is gravitational lensing. In particular, we aim to search for lensed gravitational wave signals of confirmed LIGO events from compact binary coalescences. Our major goal is to set up and test a methodology to re-identify possible lensed candidates which are initially indistinguishable from the background. We will then try to infer the intrinsic properties of the gravitational lenses by making use of the identified lensed gravitational wave signals.

In this report, Section II provides background information on the research. Section III presents the methods used and procedures in our project. Section IV gives a brief conclusion for the project. Finally, Section V discusses the future work following this project.

II. Background

A. Properties of Gravitational Waves

According to Albert Einstein's general theory of relativity in 1915 [**?**], the Universe can be perceived as a fabric of spacetime. Masses like black holes and neutron stars on this fabric produce spacetime curvature [**?**]. When masses accelerate in spacetime, they cause ripples like water waves generated when one throws a stone into water. Such ripples are known as **gravitational waves**. In this project we focus on four fundamental properties for gravitational waves as predicted by General Relativity, namely their speed, polarization, weak interaction with matter and ability to be lensed gravitationally.

The speed of gravitational waves is predicted by General Relativity to be the same as the speed of light c in vacuum [**?**]. This has been experimentally confirmed by the detection of gravitational wave from the neutron star inspiral GW170817 in 2017, which constrained the difference between the speed of light and the speed of gravitational wave to between -3×10^{-15} and $+7 \times 10^{-16}$ [**?**].

For the polarization of gravitational waves, as discussed in Ref. [**?**], we imagine placing a circular ring of test masses on the $x-y$ plane with its center coinciding with the origin. If we assume there exists a transverse - traceless (TT) gravitational wave propagating in the z-direction, then the effect of such gravitational wave is constrained to be on the $x-y$ plane only. Under the influence of the wave, the test masses ring can exhibit two orthogonal deformation modes.

As shown in Figure 1, when a **plus (+) polarized** gravitational wave passes through our ring of test masses, the

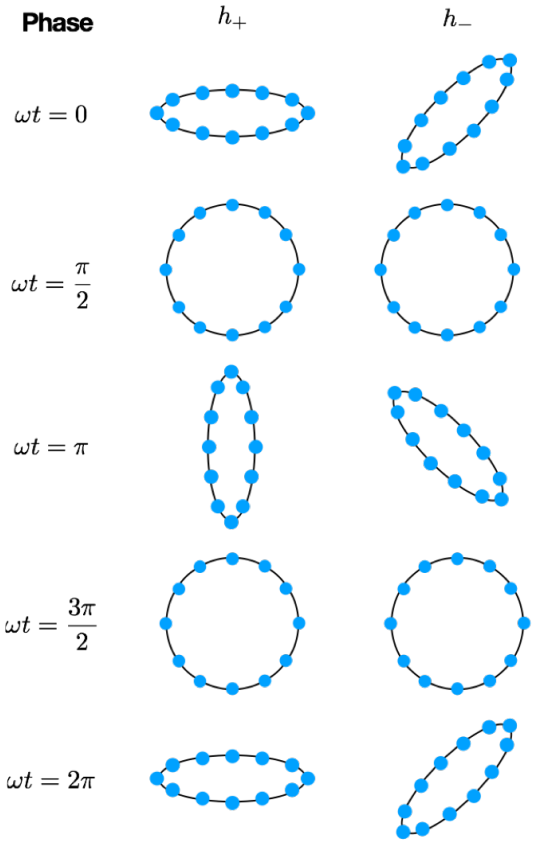

Fig. 1. Two orthogonal deformation modes within one period of the test mass ring in response to a TT-gravitational wave. The upper row refers to the plus polarization (denoted by +) and the lower row refers to the cross polarization (denoted by $\times$) of the gravitational wave. Image reproduced from [**?**].

ring is stretched along the y-direction and then along the x-direction into an ellipse of the same area as the original circle throughout one period. On the other hand, if the gravitational wave passing through is **cross** ($\times$) **polarized** instead, the ring will be stretched along the $y = x$ and $y = -x$ line in a similar way as for plus (+) polarized gravitational wave. We can see that gravitational waves can be polarized in two particular modes, namely the plus (+) polarization, and cross ($\times$) polarization. The effect of stretching and shrinking of proper lengths between test masses in the ring by polarized gravitational waves is applied to the detection of gravitational waves. In particular, detectors including LIGO and VIRGO detect gravitational waves using interferometry.

B. Detection of Gravitational Waves

A schematic overview of the gravitational wave detector used by LIGO is shown in Figure 2 [**?**]. It is a Michelson interferometer consisting of two arms, each of 4 km long. A laser beam is incident on a beam splitter, which splits the incident laser beam into two beams propagating along the two arms of the interferometer. At the end of the arm, a mirror reflects the beams which then rejoin at the beam splitter and is finally collected by a photodetector to observe the interference pattern.

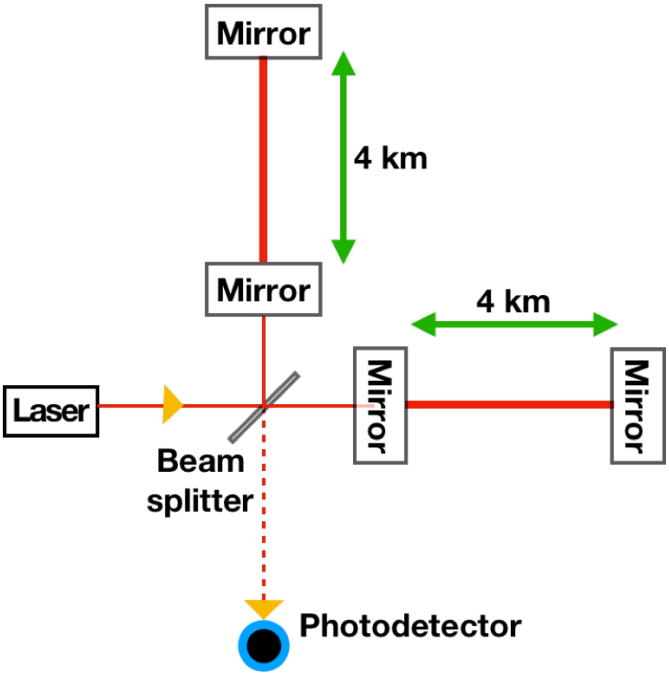

Fig. 2. A simplified schematic overview of the gravitational wave detector used by LIGO. Note that many important components of the detector, including the power and signal recycling mirrors and the input and output mode cleaners, are not shown for simplicity. Image reproduced from [**?**].

The interference of the two laser beams is set to be destructive at the photodetector. Alternatively, when there are alterations to the lengths of the arms which cause a path difference between the two laser beams, a constructive interference pattern will be observed. The change in arm lengths is not necessarily caused by gravitational waves because there is also noise which can cause such effect. These noises include seismic noises, thermal noises, gravity-gradient noises and quantum noises [**?**].

In order to detect gravitational waves, we must constrain ourselves to those which have a sufficiently large perturbation to spacetime. Typically, we focus on four types of gravitational waves, namely Continuous Waves, Stochastic Waves, Bursts and Compact Binary Coalescenes, the last one is the focus of this research. When two compact objects, for instance, neutron stars and/or black holes, orbit about their common center-of-mass, they will **inspiral** due to loss of orbital energy by means of gravitational radiation, then **merge** into a single object which then **rings down**. This sequence, "inspiral-merger-ringdown", is referred to as "coalescence". Among the four mentioned types of gravitational waves, Compact Binary Coalescences are sources of gravitational waves with well modelled waveforms compared to other kinds of gravitational wave sources, and hence one can use a technique called **matched filtering** to search for such signals.

We now outline the major steps in analyzing gravitational-wave data [**?**]. Currently, matched filtering is a method to distinguish the weak gravitational wave signals from the

detector noise fluctuations. The principle of matched filtering is to slide templates of an expected waveform from an astrophysical event across the received data and look for a strong cross-correlation between the two.

We denote $s(t)$ as the signal received from a detector, $n(t)$ as the background noise and $h(t)$ as the gravitational wave signal (if it exists). $s(t)$ is the sum of $n(t)$ and $h(t)$, that is

$$s(t) = n(t) + h(t). \tag{1}$$

If we have a filter $P(t)$, we may define

$$\hat{s} = \int s(t)P(t)dt. \tag{2}$$

We denote $\langle S \rangle$ and N as the expectation value and root mean square value of $\hat{s}$ if a gravitational wave signal is included in the data respectively. Then we have

$$\begin{aligned} \langle S \rangle &= \int \langle s(t)P(t) \rangle dt \\ &= \int \langle (n(t) + h(t))P(t) \rangle dt \\ &= \int \langle h(t)P(t) \rangle dt \\ &= \int \tilde{h}(f)\tilde{P}^*(f)df, \end{aligned} \tag{3}$$

where we have taken $\langle n(t)P(t) \rangle = 0$ (since the noise is assumed to be random and gaussian) and the tilde ($\tilde{A}$) denotes the Fourier-transform of A. Note that the last line of equation (3) is a result of Parseval's Theorem.

Also, if $h(t) = 0$, we have

$$\begin{aligned} N^2 &= \langle \hat{s}^2 \rangle - \langle \hat{s} \rangle^2 \\ &= \langle \hat{s}^2 \rangle dt \\ &= \int \int P(t)P(t') \langle n(t)n(t') \rangle dt dt' \\ &= \frac{1}{2} \int S_n(f) |\tilde{P}(f)|^2 df, \end{aligned} \tag{4}$$

where $S_n(f)$ denotes the power spectral density. We can therefore define **signal-to-noise ratio (SNR)** as

$$\begin{aligned} \rho &= \frac{\langle S \rangle}{N} \\ &= \frac{\int \tilde{h}(f)\tilde{P}^*(f)df}{\sqrt{\int \frac{1}{2} S_n(f) |\tilde{P}(f)|^2 df}}. \end{aligned} \tag{5}$$

Furthermore, we define the inner product between two functions $x(t)$ and $y(t)$ to be:

$$\langle x, y \rangle = \Re \left(\int_{-\infty}^{\infty} \frac{\tilde{x}^*(f)\tilde{y}(f)}{\frac{1}{2}S_n(f)} \right) df. \tag{6}$$

Consequently, we can have equation (5) simplified as

$$\rho = \frac{\langle d, h \rangle}{\sqrt{\langle h, h \rangle}}, \tag{7}$$

where d is the data received in the detector. With an optimal matched filter $P(t)$, and provided that the identical gravitational wave signal can be seen in coincidence between two or more detectors, LIGO detectors can detect inspiral signals with a network SNR $\rho_{\text{net}} > 8$ [**?**]. The network SNR for two or more detectors is simply calculated by adding the SNR of individual detectors in quadrature, that is

$$\rho_{\text{net}}^2 = \Sigma_i \rho_i^2, \tag{8}$$

where the index i runs over the individual detectors [**?**].

In reality, the rate of gravitational wave events occurring is expected to as low as about a few per year [**?**]. To avoid mistaking large and infrequent detector noise fluctuations mimicking events as signals, we need to find out the **false alarm rate (FAR)**, which is how often an abnormal noise signal mimicking event can be measured. The smaller the FAR is, the more plausible the candidate is a real astrophysical event. The FAR for any signal is estimated by [**?**]

$$\text{FAR} = \frac{N}{\Sigma_i T_i}, \tag{9}$$

where N is the total number of background triggers similar to the one which we consider as a real signal, and T_i is the analyzed time interval in the i^{th} background trial.

C. Gravitational Lensing

As predicted by General Relativity, since masses can curve spacetime, the path of a light ray from a source can be bent and deflected before reaching the observer (See Figure 3). Such effect is known as gravitational lensing, in the sense that it is similar to light rays being bent by optical lenses, but in this case the "lenses" are masses instead. In particular, since a source emits light rays in all direction, light rays propagating along different directions are bent differently and may, therefore, form multiple images. The images can vary in arrival time and amplitudes.

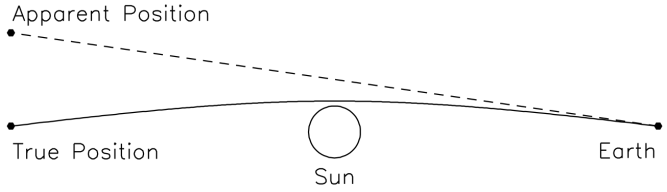

Fig. 3. Light rays from a source are bent because of a gravitational lens in between the source and the observer. Image from [**?**].

In fact, according to Einstein's equivalence principle [**?**], all electromagnetic waves, as well as all gravitational waves, will be gravitationally lensed in the same way, and this phenomenon has been observed on astronomical scales for light and gravitational waves of all wavelengths. However, the study of gravitational lensing of light encounters difficulties from the blocking of light by dust clouds in the Universe, as well as the large noise which screened the light

signals [**?**]. General relativity also predicts that gravitational waves, having a similar nature as light, can also be lensed gravitationally, producing multiple signals, and same as light, is achromatic. In contrast to light, gravitational waves are not disturbed by the dust clouds between the source and observing point.

Over the past two years, more than six gravitational wave detections have been successfully made [**?**], [**?**], [**?**], [**?**], [**?**], [**?**], which have confirmed the prediction of the existence of gravitational waves and permitted new tests of General Relativity in the strong field regime and make it possible to study the properties of the sources, including masses, spins and merger rates. Among the four predicted fundamental properties of gravitational waves, which are their speed, polarization, weak interaction with matter and ability to be lensed gravitationally, that we mentioned at the very beginning of Section II, we are only left with the last one - ability to be gravitational lensed, untested. Therefore, it is now the right time for us to start searching for lensed gravitational wave signals so as to test this property of gravitational wave predicted from general relativity.

Due to lensing, there are time delays among the waves of lensed events. In the discussion for electromagnetic waves, there are two major contribution to the delay, namely refraction and gravitational time delay. Gravitational lensing occurs when light rays pass through spacetime perturbed by masses. This will form multiple signals which differ in amplitude and time of arrival. The difference in arrival time is due to 1) The path lengths travelled from the images to the observer vary, and 2) The effective speed of light can be different under the influence of a refractive index larger than one, resulting in arrival time delay.

The same thing happens with gravitational waves, except that their weak interaction with matter means that the refractive index is negligibly different from one. Therefore, the only crucial effect to account for is the geometric effect, which causes both magnification and time delay of lensed signals. An important point to note here is that there is no dispersion, and hence the geometric lensing is achromatic. That is to say, it affects all frequency components of the wave in exactly the same way.

In the derivations below, for cosmological distances, they are referred to as the angular diameter distances. As shown in Figure 4, the angular diameter distances from the observer to the lens and the source are given by D_L and D_S respectively, and that from the source to the lens is D_{LS}. When we compare the path difference between the unperturbed ray (dotted line between the observer and the source in figure 4), that is when the lens is absent, and the lensed ray (solid lines between the observer and the source), we have [**?**]

$$\vec{\xi} = \frac{D_L D_{LS}}{D_S}(\vec{\theta} - \vec{\theta_S}), \tag{10}$$

where ξ is the separation between the two rays at the lens, $\vec{\theta}$ is the two-dimensional angle between the horizontal of the observer and the point where the gravitational waves strike the lens, and $\vec{\theta}_S$ is the angle between the horizontal of the observer and the source.

With this, we have the geometrical path difference ΔD between the unperturbed ray and lensed ray is given by

$$\Delta D = \frac{\vec{\xi}(\vec{\theta} - \vec{\theta_S})}{2}. \tag{11}$$

Finally, the geometrical time delay Δt due to gravitational lensing is given by

$$\Delta t = (1 + z_d)\frac{D_L D_{LS}}{2 D_S c}(\vec{\theta} - \vec{\theta_S})^2, \tag{12}$$

where z_d denotes the gravitational redshift. From the calculation of the time delay, we are able to infer the distance of the lens from the observer.

For gravitationally lensed gravitational wave signals, the lensed waveform has an amplitude $h^{\text{lensed}}_{+,\,\text{x}}(f)$ given by [**?**], [**?**]

$$h^{\text{lensed}}_{+,\,\text{x}}(f) = F(\omega, y) h^{\text{unlensed}}_{+,\,\text{x}}(f), \tag{13}$$

where $h^{\text{unlensed}}_{+,\,\text{x}}(f)$ denotes the amplitude of the unlensed gravitational waves, and $F(\omega, y)$ is the amplification function given by

$$F(\omega, y) = \exp\left[\frac{\pi\omega}{4} + i\frac{\omega}{2}\left(\ln\left(\frac{\omega}{2}\right) - \frac{\sqrt{y^2+4} - y^2}{4} + \ln\left(\frac{\sqrt{y^2+4}+y}{2}\right)\right]\Gamma\left(1 - \frac{i}{2}\omega\right) \times_1 F_1\left(\frac{i}{2}\omega, 1; \frac{i}{2}\omega y^2\right), \tag{14}$$

where $h^{\text{lensed}}_{+,\,\text{x}}(f)$ is the waveform without lensing, Γ is the complex gamma function, ${}_1F_1$ is the confluent hypergeometric function of the first kind, $\omega = 8\pi M_{\text{Lz}} f$; $M_{\text{Lz}} = M_{\text{L}}(1+z_L)$ is the redshifted lens mass, $y = \frac{D_L S}{\Xi_0 D_S}$ is the source position, $\Xi_0 = (\frac{4M_L D_L D_{\text{LS}}}{D_S})^{\frac{1}{2}}$ is a normalisation constant, and M_L and z_L are the lens mass and redshift respectively. From finding the amplitude of the lensed gravitational waves, we can infer both the mass M_L and the position of the lens.

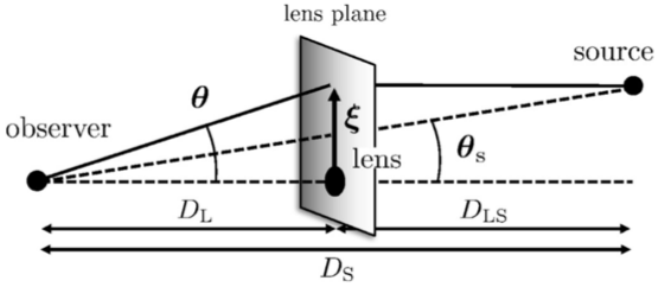

Fig. 4. In this figure, D_L denotes the distance between the lens and the observer, D_S denotes the distance between the observer and the image, D_{LS} denotes the distance between the lens and the image, $\vec{\theta}$ denotes the two dimensional angle between the observer and lensing point, and $\vec{\theta_s}$ denotes the two dimensional angle between the source and the observer. Note that θ and θ_{s} are both two-dimensional angles. Image from [**?**].

Consider a point mass lens, particularly for compact objects like black holes or stars. In the geometrical optics limit ($f >> M_{\rm Lz}^{-1}$) from the equation above, we have [**?**]

$$F(\omega, y) = |\mu_+|^{1/2} - i|\mu_-|^{1/2} e^{2\pi i f \Delta t_d}, \tag{15}$$

where the magnification of each image is

$$\mu_\pm = \frac{1}{2} \pm \frac{(y^2+2)}{2y\sqrt{y^2+4}}, \tag{16}$$

and the time delay between the double images is

$$\Delta t_d = 4M_{\rm Lz}\left[\frac{y\sqrt{y^2+4}}{2} + ln\left(\frac{\sqrt{y^2+4}+4}{\sqrt{y^2+4}-y}\right)\right]. \tag{17}$$

The typical time delay for the point mass lens is therefore $2 \times 10^3 s \times \left(\frac{M_L}{10^8 M_\odot}\right)$. Furthermore, for gravitational waves from coalescence of super massive black holes of mass $10^4 - 10^7 M_\odot$ under the lensing effect of a point mass lens of mass in the range $10^6 - 10^9 M_\odot$, then the typical time delay will be $10 - 14s$ [**?**]. Therefore, for gravitational waves from blackholes of masses lower than $10^4 M_\odot$, we would expect a time delay in the range $10^1 - 10^3$s.

III. Methods and Procedures

A. GstLAL search pipeline

This research is based on the use of GstLAL search pipeline [**?**]. Figure 5 shows the schematic flow of the pipeline.

B. Searching for possible lensed candidates for GW150914 in O1 and O2 using LALInference posterior data

We make use of LALInference software library [**?**] posterior data analysis of the event GW150914. The following table shows the posterior estimation of the parameters of the two black holes involved in GW150914:

Parameter	Maximum Posteriori (maP)	Variation (σ)
$m_{1,\rm source}$	$32.9 M_\odot$	$4.9 M_\odot$
$m_{2,\rm source}$	$13.7 M_\odot$	$3.5 M_\odot$
$a_{1,\rm z}$	-0.618	0.218
$a_{2,\rm z}$	0.083	0.243

where $m_{1,\rm source}$, $m_{2,\rm source}$, $a_{1,\rm z}$ and $a_{2,\rm z}$ are the respective masses and components of spins aligned with the orbital angular momentum of the binary blackhole system of the two black holes in GW150914 evaluated by the LALInference library. Using the information, we search for triggers throughout O1 and O2 with masses and spins within 3 and 4σs from the maP of GW150914 which are regarded as possible lensed candidates for the event. Figure 6 to 9 show the search results for O1 and O2 within 3σ range and 4σ range. Note that μ on the y-axis refers to the magnification of the triggers comparing to GW150914, which is evaluated by:

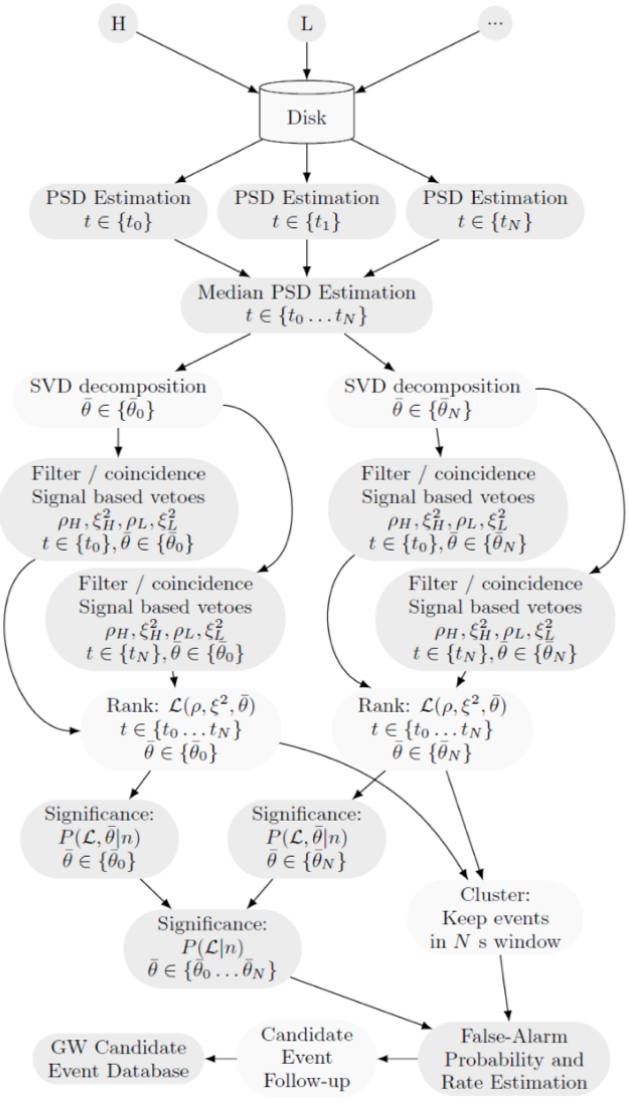

Fig. 5. A schematic flow of the GstLAL search pipeline. Image from [**?**].

$$\mu = \frac{\text{Signal-to-noise ratio of found trigger}}{\text{Signal-to-noise ratio of GW150914}}, \tag{18}$$

and the relative time delay on the x-axis refers to the time delay of the found triggers relative to the geocentric arrival time of GW150914, which is $1126259462s$ [**?**] (The corresponding UTC time is 2015-09-14 09:50:45). The colours of the dots indicate the likelihood, a measure of the distinguishability of the event from the detector noise, of the triggers.

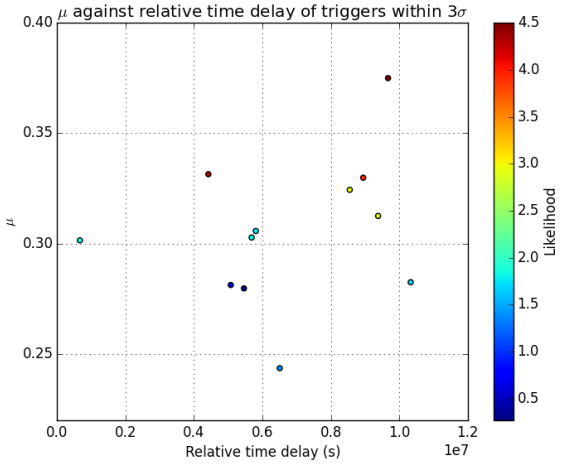

Fig. 6. Searched triggers in O1 with parameters within 3σ range from GW150914.

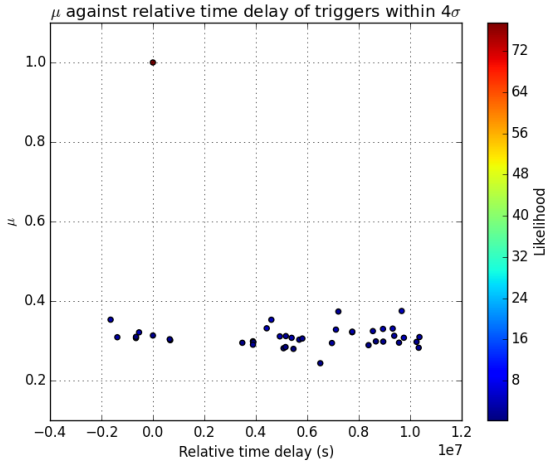

Fig. 8. Searched triggers in O1 with parameters within 4σ range from GW150914. Note that the detected GW150914 event is visible at relative time delay = 0 and μ = 1

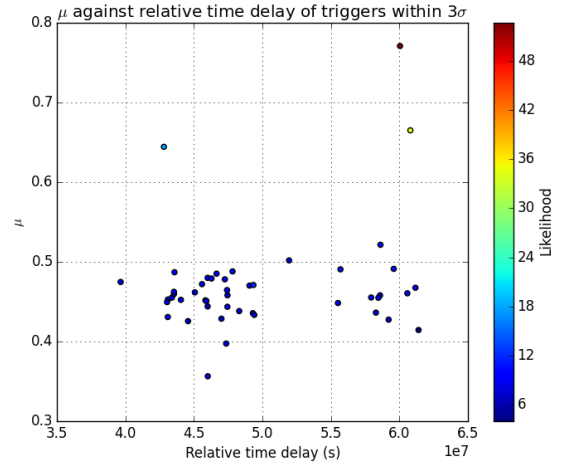

Fig. 7. Searched triggers in O2 with parameters within 3σ range from GW150914.

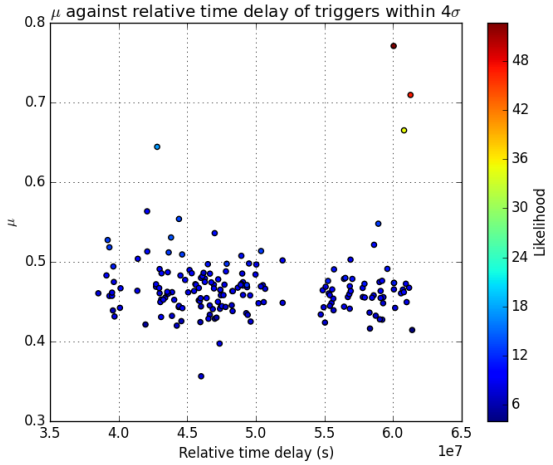

Fig. 9. Searched triggers in O2 with parameters within 4σ range from GW150914.

Remarks on the method

We note that the trigger, which is a candidate event where the SNR $\rho(t)$ peaks in time above a certain threshold, corresponding to GW150914, which should have $\mu = 1$ and Relative time delay = 0, does not show up in the 3σ range plot in O1, and it only shows up when we loosen the range to 4σ. This is due to the inconsistency of data used between LALInference and GstLAL. In fact, LALInference is designed to accurately infer the parameters of the source, while GstLAL is not. Therefore, their results are not completely agreeing with each other, leading to the absence of GW150914 in the 3σ plot.

Also, we are aware that the signal-to-noise ratio (SNR) evaluated in both O1 and O2 may have discrepancies since the background noise is varying every moment. Initially, we proposed looking into the power spectral density in O1 and O2 to link the SNRs, but we decided to do better and hence this method is called off.

C. Searching for possible lensed candidates for GW150914 in O1 and O2 using GstLAL data

Regarding the problems in the previous method, we rerun the search by using GstLAL data. The following table shows the GstLAL parameter data regarding the event GW150914 [**?**]:

Parameter	Value
Mass 1	$47.9M_{\odot}$
Mass 2	$36.5M_{\odot}$
Spin 1 (along z-direction)	0.962
Spin 2 (along z-direction)	-0.900
Chirp mass	$33.8M_{\odot}$

Using similar techniques from the last method, we search through O1 to look for triggers with mass 1 and mass 2 within a certain percentage range of the chirp mass. The objective is to find a distinctive feature for separating possible lensed triggers from the background. Figure 10 - 14 show the results for 10%, 30% and 50% chirp mass range.

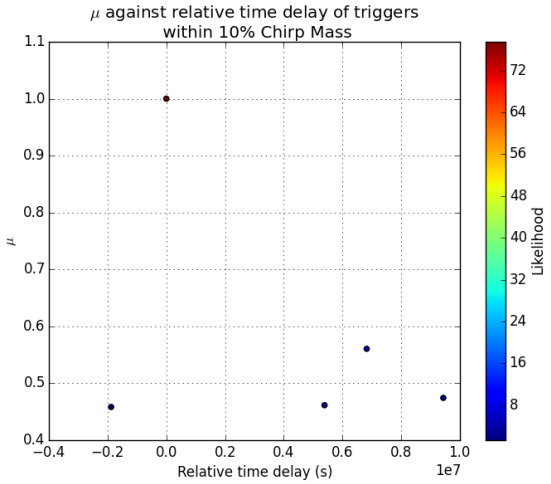

Fig. 10. Searched triggers in O1 with mass 1 and mass 2 within 10% chirp mass range from GW150914.

We note that all of the triggers in the search have likelihood smaller than 20, except for the detected GW150914 event which has a likelihood above 70.

Remarks on the method

Although some triggers appear to be distinguishable from the background cluster in the 30% and 50% plots, the magnification of those triggers is unexpectedly high (up to 0.7) considering the exceptionally high SNR of GW150914. A possible reason behind is our neglecting of χ^2 for the detection. We decided to shelve this method and to obtain a distribution of the likelihood of possible lensed triggers as our next step.

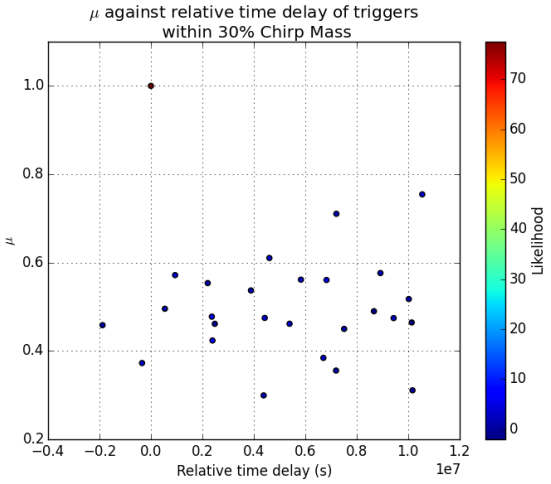

Fig. 11. Searched triggers in O1 with mass 1 and mass 2 within 30% chirp mass range from GW150914.

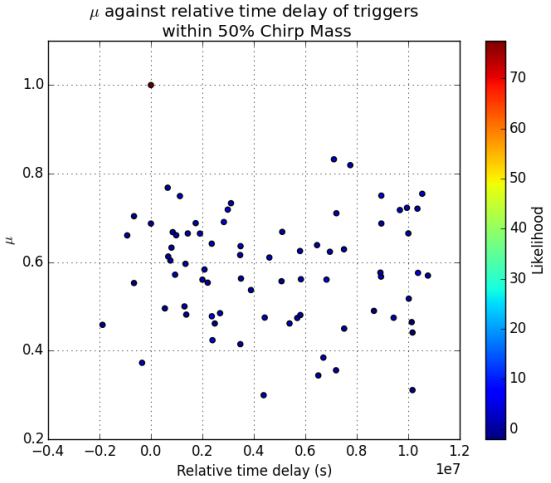

Fig. 12. Searched triggers in O1 with mass 1 and mass 2 within 50% chirp mass range from GW150914.

D. Searching for possible lensed candidates for GW150914, GW170608 and GW170814 in O1 and O2 using unclustered GstLAL data

We aim to retrieve a likelihood distribution of lensed gravitational wave signals at this stage. The objective of doing so is to figure out the range of parameters and templates to use to search for them. We will form a template bank which is much smaller than the full bank used to search for any binary coalescence signal capable of of being detected by the LIGO detectors. It is expected that the event-count vs ranking statistic threshold curve will be shifted downward for lensed triggers, as shown in Figure 13, since in our gstLAL run, the background noise distribution is not from the entire template bank, but instead from a much smaller template bank, and therefore produces much less background, which allows us to do a targeted search for the lensed gravitational wave signals. This is the major reason why we are launching the injection campaign in the later stage of our project.

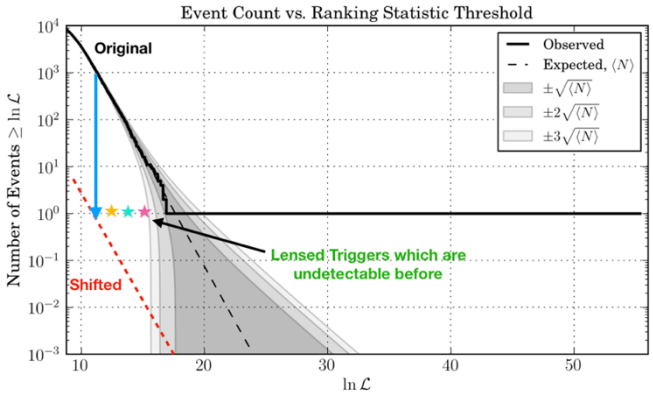

Fig. 13. Expected event-count vs ranking statistic threshold curve for lensed gravitational wave signals, using GW170608 as an example. Note that the shifted red event-count vs ranking statistic threshold curve, and also the stars denoting the lensed triggers we expect to find, are only for illustrative means. In other words, they are not actual data.

We rerun part of the GstLAL run jobs and obtain the unclustered data for each focused event. We then obtain templates around the time of the event and select those with SNR higher than 70% of the maximum. We search through the chunk in which the event happened to find triggers which match the parameters (mass 1, mass2, spin1z, spin2z) in our template bank exactly and regard them as possible lensed triggers. Finally, we plot the distribution of the likelihood of the triggers and compare it with the event-count vs ranking statistic threshold graph. Figure 14 - 17 show the results for GW150914, GW170608 and GW170814. In each of the figures, one sees the solid black line (observed) and the dashed line (expected) indicating the event-count vs ranking statistics threshold curve with the background from the entire template bank. The curve with background from the much smaller template banks we used for our search is not yet to be known. The blue bar(s) in the middle and/or right side of each graph corresponds to the detected event, while those on the left refer to some found triggers with very low likelihood from our search. We hope to get a sense of how the likelihood distribution for lensed gravitational wave signals would look like from these searches.

Remarks on the method

From the plots, we can already get a sense of how the distribution of the likelihood of possible lensed triggers will be. However, we are still uncertain about the searching range of parameters (reduced template bank) for possible lensed triggers. Until now, we are still varying the SNR percentage threshold to determine a reduced templated bank and get a satisfactory result. A more systematic way to actually obtain the likelihood distribution of lensed candidates will be to run an injection campaign, which is done in Week 4 - 6 of the SURF period.

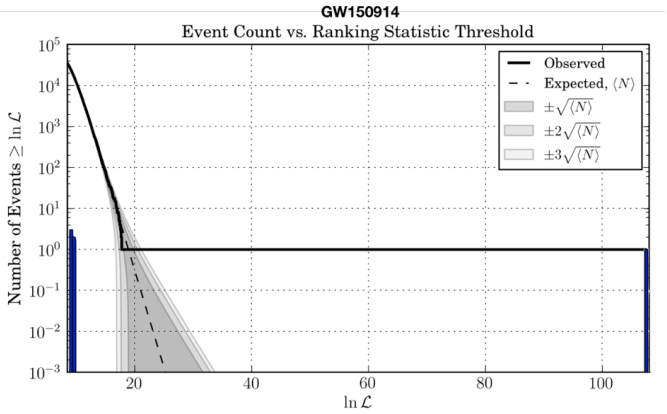

Fig. 14. Distribution of likelihood (blue bars) of searched matching triggers in O1-chunk1 using raw data for the event GW150914. Note that the barely visible blue bar on the right boundary corresponds to the detection of the event GW150914.

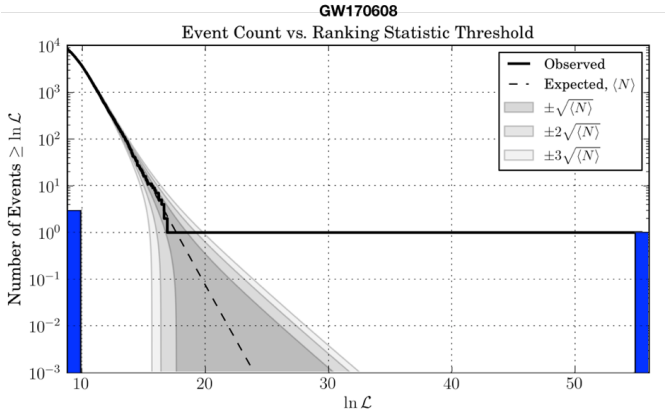

Fig. 15. Distribution of likelihood (blue bars) of searched matching triggers in O2-chunk-GW170608 using raw data for the event GW170608. The blue bar on the right boundary corresponds to the detection of the event GW170608.

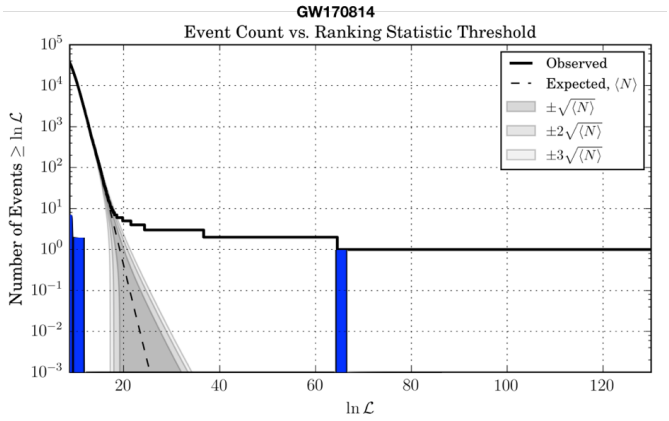

Fig. 16. Distribution of likelihood (blue bars) of searched matching triggers in O2-chunk21 using raw data for the event GW170814. The blue bar in the middle refers to the detection of the event GW170814. Note that the solid (observed) event-count versus ranking statistics threshold curve extends beyond the middle blue bar instead of stopping there, since there is another detection, which is GW170817, in the same chunk we are analysing here.

E. Preparation work for running an injection campaign

Following the last part, we attempt to run an injection campaign to obtain a likelihood distribution of lensed gravitational wave signals. From this, we can identify a set of templates for use in a reduced template bank for a "targeted" search. The first step is to read in the LALInference posterior samples [**?**]. Table 1 below shows the important items in each of the LALinference posterior sample file (using GW150914 - allSsp_post.dat as a sample).

TABLE I
A TABLE SHOWING THE IMPORTANT ELEMENTS IN EACH OF THE LALINFERENCE POSTERIOR SAMPLE FILE.

Item	Content [**?**]
l1_end_time	Reference time at Livingston site (time of coalescence / peak amplitude)
v1_end_time	Reference time at VIRGO site (time of coalescence / peak amplitude)
h1_end_time	Reference time at Hanford site (time of coalescence / peak amplitude)
time	Reference time at geocentre (time of coalescence / peak amplitude)
m1	Mass of the primary object (detector frame)
m2	Mass of the secondary object (detector frame)
a1z	The z-component of spin of the primary object
a2z	The z-component of spin of the secondary object
mc	Chirp mass (detector frame)
distance	Distance to source
dec	Declination of the gravitational wave source
ra	Right ascension of the gravitational wave source
psi	Polarisation angle (3^{rd} Euler angle) required to transform the tensor perturbation in the radiation frame to the detector frame
costheta_jn	Cosine of the angle between the total angular momentum and the line of sight vector
theta_jn	Angle between total angular momentum and line of sight
eta	Symmetric mass-ratio
optimal_snr	Optimal Signal-to-Noise Ratio (SNR) of the model
logl	Natural log of the likelihood
lal_amporder	Post Newtonian amplitude order

Next, we try to make an injection file with a sim_inspiral table containing simulated lensed signals of GW150914 which we produced from the posterior samples. The transfer of information from the posterior samples to the generated sim_inspiral table is not straightforward and some items require re-calculations. The technical details may be found in the attached code files. Table 2 lists the important items in the sim_inspiral table and the related posterior samples' items.

TABLE II
A TABLE SHOWING THE IMPORTANT ELEMENTS IN SIM_INSPIRAL TABLE AND THE RELATED POSTERIOR SAMPLES' ITEMS.

Item	Content and related posterior samples items
h_end_time	Reference time at Hanford site (time of coalescence / peak amplitude) [Integral value] **Related item(s) :** h1_end_time
h_end_time_ns	Reference time at Hanford site (time of coalescence / peak amplitude) [Nanosecond] **Related item(s) :** h1_end_time
l_end_time	Reference time at Livingston site (time of coalescence / peak amplitude) [Integral value] **Related item(s) :** l1_end_time
l_end_time_ns	Reference time at Livingston site (time of coalescence / peak amplitude) [Nanosecond] **Related item(s) :** l1_end_time
v_end_time	Reference time at Virgo site (time of coalescence / peak amplitude) [Integral value] **Related item(s) :** h1_end_time
v_end_time_ns	Reference time at Virgo site (time of coalescence / peak amplitude) [Nanosecond] **Related item(s) :** h1_end_time
geocent_end_time	Reference time at geocentre (time of coalescence / peak amplitude) [Integral value] **Related item(s) :** time
geocent_end_time_ns	Reference time at geocentre (time of coalescence / peak amplitude) [Nanosecond] **Related item(s) :** time
mass1	Mass of the primary object (detector frame) **Related item(s) :** m1
mass2	Mass of the secondary object (detector frame) **Related item(s) :** m2
mchirp	Chirp mass (detector frame) **Related item(s) :** mc
spin1z	The z-component of spin of the primary object **Related item(s) :** a1z
spin2z	The z-component of spin of the secondary object **Related item(s) :** a2z
distance	Distance to source **Related item(s) :** distance, ra, dec, optimal_snr
longitude	Right ascension* of the gravitational wave source **Related item(s) :** ra
latitude	Declination* of the gravitational wave source **Related item(s) :** dec
eta	Symmetric mass-ratio **Related item(s) :** eta
inclination	angle between total angular momentum and line of sight **Related item(s) :** theta_jn
polarization	Polarisation angle (3^{rd} Euler angle) required to transform the tensor perturbation in the radiation frame to the detector frame **Related item(s) :** psi
amp_order	Post Newtonian amplitude order **Related item(s) :** lal_amporder

Following [**?**], the quantity

$$\rho(t) = \frac{|z(t)|}{\sigma} \tag{19}$$

is the amplitude signal-to-noise ratio of the (quadrature) matched filter, where σ is a measure of the sensitivity of the detector to a signal with waveform $h_1(f)$ defined by

$$\sigma^2 = 4\int_0^\infty \frac{\tilde{h}_1(f)}{S(f)} df \tag{20}$$

with $\tilde{h}_1$ being the signal and $S(f)$ being the power spectral density, and

$$z(t) = 4\int_0^\infty \frac{\tilde{s}(f)[\tilde{h}^*(f)]}{S(f)} e^{2\pi i f t} df \tag{21}$$

is the modulus of the complex filter output, with $s(f)$ following the definition in equation (1). With such, a biased estimate of the **effective distance** to the candidate system is

$$D_{\text{eff}} = \left(\frac{\sigma}{\rho}\right)\text{Mpc}. \tag{22}$$

We generate simulated lensed signals by altering the effective distance of the samples with equation (22).

Remarks

A challenge to generating simulated lensed signals is that the samples store only "distance" D instead of "effective distance" D_{eff}, and both of them depend on the sky location (i.e. right ascension $alpha$ and declination δ) of the source. Particularly, the relationship between D and D_{eff} is given by

$$D_{\text{eff}} = D\left[F_+^2\left(\frac{1+cos^2\iota}{2}\right)^2 + F_\times^2\left(cos^2\iota\right)\right]^{-\frac{1}{2}}, \tag{23}$$

where F_+ and $F_\times$ are the antenna response functions for the signal. The resolution to this is to make use of the *ComputeDetAMResponse* from the *lal* python package to compute the values of F_+ and $F_\times$.

F. Running the injection campaign

We substitute information (mass1, mass2, spin1z, spin2z, distance) of the original injection file by those of our simulated lensed signals. Using the modified injection file, we rerun the GstLAL run to search for the injected lensed signals.

Remarks

The clusters have been problematic and slow over the time we are running the injection campaign. There are moments when we cannot even log-into the clusters. According to the people managing the clusters, they are either encountering internet issues or hardware issues. We also suspect that the problems are attributed to the current integration of KAGRA members into the clusters. To resolve the problem, we do a shortcut GstLAL run by reducing the injection time range from the full observation chunk to a week time. We expect this will help to make the jobs complete quicker. Although the result may not be perfect, it will still be decent and satisfactory. The full injection runs will be done as future work. See Section IV for more information.

We have successfully completed a full injection run for GW150914 and a shortcut injection run for GW151226 throughout the SURF period. The figures below show the distance at which you should see a lensed signal for GW150914 / GW151226. The first panel shows the time evolution of the horizon distance and the second panel shows the same information in histogram form.

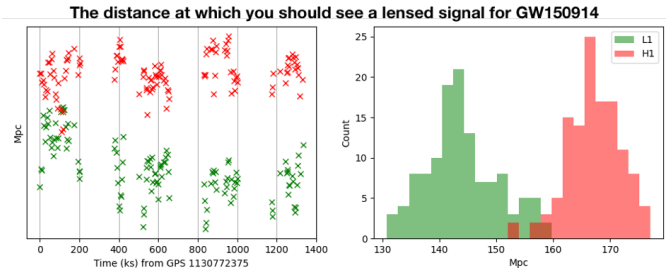

Fig. 17. The distance at which you should see a lensed signal for GW150914.

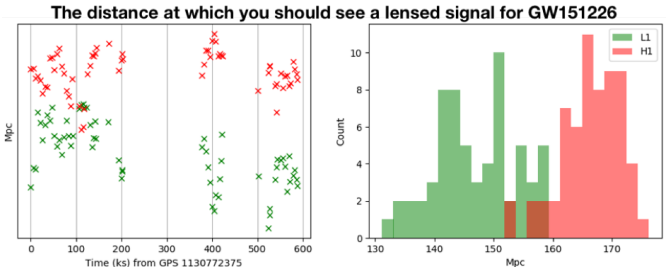

Fig. 18. The distance at which you should see a lensed signal for GW151226.

Note that when we generate simulated lensed signals, we **choose to** constrain the SNR of each signal to have a minimum SNR of 4. For each sample, within the range of SNR 4 to the original SNR of the sample, we generate 10 injections with SNR uniformly distributed in the range by altering their effective distances. From equation (22) we see that

$$\rho \propto \frac{1}{D_{\text{eff}}}, \tag{24}$$

and hence by altering the SNR ρ of the signal we have

$$d\rho \propto \frac{dD_{\text{eff}}}{D_{\text{eff}}^2}. \tag{25}$$

This relationship is reflected from the histogram shown on the right side of Figure 18. If we choose another way to generate our simulated signals, for instance,

$$\rho^2 \propto \frac{1}{D_{\text{eff}}^2}, \tag{26}$$

the distribution shown in the histogram will be different.

After the gstLAL run completed, we search through the chunk in which the event happened to find triggers which match the parameters (mass 1, mass2, spin1z, spin2z) of our recovered templates exactly and regard them as possible lensed triggers. Finally, we plot the distribution of the likelihood of the triggers and compare it with the event-count vs ranking statistic threshold graph. Figure 20-21 show the results for GW150914 and GW151226. In each of the figures, one sees the solid black line (observed) and the dashed line (expected) indicating the event-count vs ranking statistics threshold curve with the background from the entire template bank. The curve with background from the much smaller template banks we used for our search is not yet to be known. The blue bar(s) on the left refer to the found triggers with very low likelihood from our search.

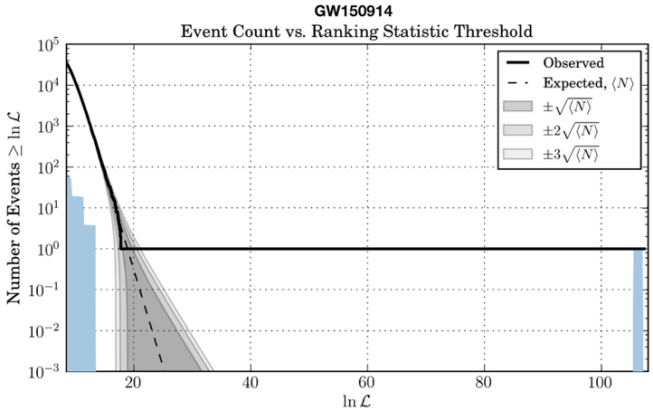

Fig. 19. Searched triggers in O1 Chunk 5 with parameters (mass1, mass2, spin1z, spin2z) matching those of the simulated lensed signals templates for GW150914 recovered from the injection run. Note that the right blue bar, representing the detected event GW150914, is still visible in the graph.

As we can see from figure 20 and 21, we have already successfully lowered the background noise by using a much smaller template bank for our lensed gravitational wave signal search. We have also added a red dashed line in Figure 21 as our expectation of the shifted event-count vs ranking statistic threshold curve to illustrate the idea. For our next step, we will use the recovered triggers as the simulated lensed signal templates and do a gstLAL run search to search for possible lensed candidates in the data.

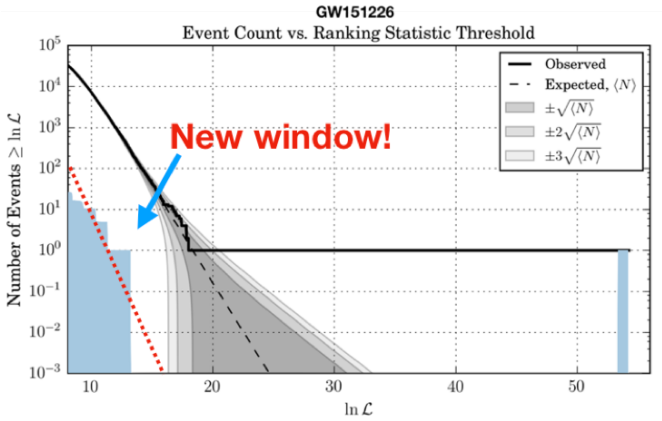

Fig. 20. Searched triggers in O1 Chunk 8 with parameters (mass1, mass2, spin1z, spin2z) matching those of the simulated lensed signals templates for GW151226 recovered from the injection run. Note that the right blue bar, representing the detected event GW151226, is still visible in the graph. The red dashed line is the expected event-count vs ranking statistic threshold curve, and it is only for illustrative means. In other words, they are not actual data. However, we can already see that our injection run can open a new window, as shown by the space between the red shifted curve and the original black dashed curve, to search for lensed gravitational wave signals.

G. Literature review on gravitational lensing of gravitational waves

We follow the mathematics and approach of [**?**] to compute the probability distribution of relative time delays and magnification of lensed gravitational wave signals through a singular isothermal ellipsoid (SIE) lens model. Singular isothermal ellipsoid (SIE) lens models have a surface mass density which diverges at the center. These lenses can produce either two or four images. The lens model itself has two parameters, namely the velocity dispersion σ and the axis-ratio q. We follow [**?**] to generate these parameters with distribution taken from the SDSS galaxy population. The following figures shows the reproduced results (Figure 24 and 25) compared to the original results shown in [**?**] (Figure 22 and 23).

We have reproduced a probability distribution function of relative time delay δt and magnification of lensed gravitational wave signals that is very similar to what was presented in [**?**]. We noted from Figure 22 that for most of the the lensed gravitational wave signal with highest amplitude(μ_1), they have magnification larger than 1. Regarding this model, this suggests that most of our detected events, like GW150914, could possibly be lensed versions of their original (unlensed) signals. If this is indeed the case, then by neglecting the possibility of magnification, we have over-estimated the amplitude of our signals, and thus underestimated the luminosity and redshift of these signals. This would also lead to an over-estimate of the source massess.Therefore, if we are to use the model results, we will have to look for unlensed version of the detected event instead.

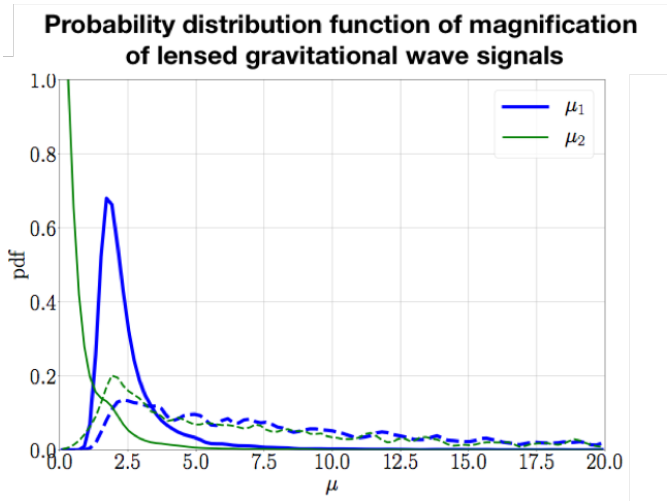

Fig. 21. Probability distribution of magnification μ_1 and μ_2 of the two dominant lensed gravitational wave signals from the study present in [**?**]. The Solid (dashed) traces show distributions before (after) applying the detection threshold SNR > 8. The component masses of the simulated events are sampled from power law 1 distribution.

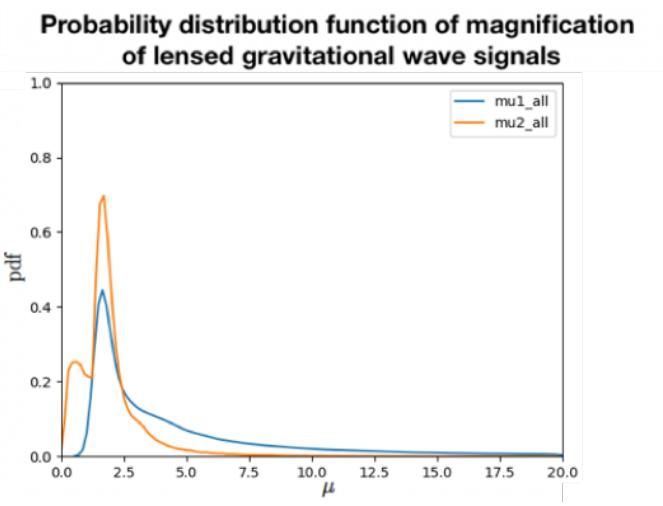

Fig. 23. Probability distribution of magnification μ_1 and μ_2 of the two dominant lensed gravitational wave signals reproduced by myself. The Solid (dashed) traces show distributions before (after) applying the detection threshold SNR > 8. The component masses of the simulated events are sampled from power law 1 distribution.

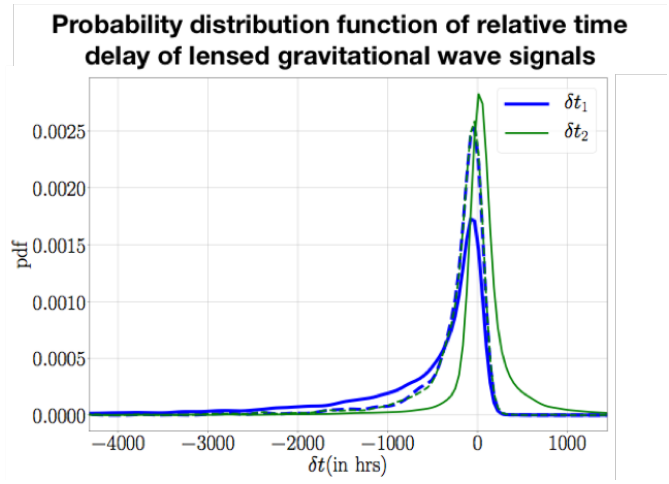

Fig. 22. Probability distribution function of relative time delay δt_1 and δt_2 of the two dominant lensed gravitational wave signals from the study present in [**?**]. The Solid (dashed) traces show distributions before (after) applying the detection threshold SNR > 8. The component masses of the simulated events are sampled from power law 1 distribution.

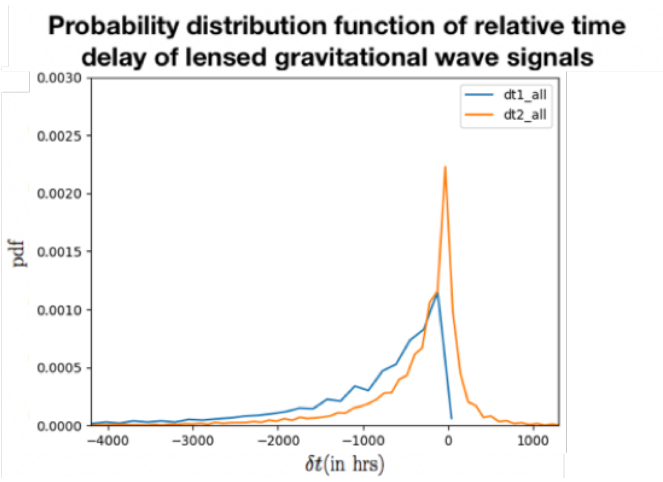

Fig. 24. Probability distribution function of relative time delay δt_1 and δt_2 of the two dominant lensed gravitational wave signals reproduced by myself. The Solid (dashed) traces show distributions before (after) applying the detection threshold SNR > 8. The component masses of the simulated events are sampled from power law 1 distribution.

After the whole injection campaign is finished, we can make use of these probability distributions to help us determine the probability that each searched candidate is a lensed (unlensed) version of the original detected event. We have also approached the researchers of [**?**] and they agreed that we can collaborate on this project.

IV. Conclusions

In this project, we used various targeted search methods to lower the background noise in order to uncover possible lensed / unlensed gravitational waves. The initial methods including using LALInference posterior data and gstLAL posterior data for searching are not good-enough methods. We end up using the injection campaign method for the detected events GW150914 and GW151226 and have successfully lowered the background, which opens up a new window for us to search for lensed / unlensed gravitational wave signals. We have also reproduced the probability distribution of relative time delays and magnification of lensed gravitational wave signals through a singular isothermal ellipsoid (SIE) lens model, which suggests that, given the model is correct, most of the lensed gravitational wave signals would have magnification larger than 1 and hence most of the detected events so far could actually be lensed version of their originals. Nevertheless, this still depends on whether there is a significant gravitational lens between us (the observer) and the source of gravitational wave, which we will have to further work on after this project.

V. Future Work

A. Completing the injection campaign for GW150914

We have already produced a much smaller template bank for lensed / unlensed version of the detected event GW150914. We will use our template bank and do a full gstLAL search run to look for possible lensed / unlensed candidates of GW150914.

B. Running injection campaign for other detected events

We have almost completed full injection run for the event GW150914. We will also conduct the full injection run for other detected events including GW151226, LVT151012, GW170104 and GW170608, GW170814 and GW170817.

C. Inferring the properties of the gravitational lens

Once we identify lensed gravitational wave signals, we will go on and try to infer some properties of the gravitational lens, including its mass, the lens-observer distance and the lens-source distance. The parameters inference step requires further literature review on gravitational lensing and involves more calculations. Alternatively, we may try to use available lens models, like in Section V we follow [**?**] to reproduce the results for probability distribution of relative time delay and magnification of lensed gravitational wave signals under the influence of a singular isothermal ellipsoid (SIE), to check how likely the identified triggers are under the effect of the proposed models. We may also consider making use of the package LENSTOOLS [**?**], which is being widely used for lens optimisation in studying gravitational lensing.

D. Using galaxy cluster / supercluster catalogue

We will try to make use of the available galaxy cluster / supercluster catalogue to verify the presence of possible gravitational lens between the detectors and the source once lensed gravitational wave signals are identified.

E. Pipelining the search for lensed gravitational wave signals

To make the search for gravitational wave signals efficient, we may try to construct a pipeline (makefile) for the search. This can make the process more time-efficient, and it will also make error-finding easier.

F. Re-introducing the sky location problem to the project

We have neglected the alteration in sky location of the source when we inject simulated lensed signals using LALInference posterior samples in this project. In particular, we need to investigate the range of sky location to search for lensed gravitational wave signal, instead of using the range suggested by LALInference. Figure 24 illustrates the problem.

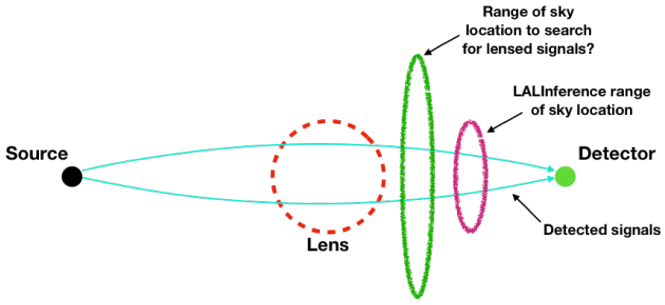

Fig. 25. An illustration of the sky-location problem on the project.

We will try to estimate the deflection angle for lensed gravitational wave signals in the future. Yet, it is important to note that the sky-location deflection addressed here is known to be small (much less than a degree) even for large lenses, especially when compared with the sky-localization capabilities of the LIGO-Virgo detector network.

We will also try to find the correlation between the relative time delay δt of lensed gravitational wave signals and the corresponding sky-location of the source (i.e. right ascension α and declination δ), or even trace the lensed gravitational wave signals.

VI. Acknowledgement

The author would like to thank Professor Alan Weinstein, Professor Tjonnie Li, Surabhi Sachdev and Rico Lo Ka Lok for their guidance and help throughout this project, and Caltech SFP and CUHK Physics for granting the research opportunity.